JOURNAL OF SPACECRAFT AND ROCKETS
Vol. 45, No. 5, September–October 2008

Time-Accurate Numerical Prediction of Free-Flight Aerodynamics of a Finned Projectile

Jubaraj Sahu*
U.S. Army Research Laboratory, Aberdeen Proving Ground, Maryland 21005-5066

DOI: 10.2514/1.34723

This article describes a new multidisciplinary computational study undertaken to compute the flight trajectories and simultaneously predict the unsteady free-flight aerodynamics of a finned projectile configuration. Actual flight trajectories are computed using an advanced coupled computational fluid dynamics/rigid body dynamics technique in a body-fixed coordinate system. An advanced time-accurate Navier–Stokes computational technique has been used in computational fluid dynamics to compute the unsteady aerodynamics associated with the free flight of the finned projectile at supersonic speeds. Computed positions and orientations of the projectile have been compared with actual data measured from free-flight tests and are found to be generally in good agreement with the data. Predicted aerodynamics forces and moments also compare well with the forces and moments used in the 6 degree of freedom fits of the results of the same tests. Unsteady numerical results obtained from the coupled method show the flowfield, the aerodynamic coefficients, and the flight paths of the projectile.

Nomenclature

C_{lp}	=	roll damping moment coefficient normalized by $(pd/2V)$
C_m	=	pitching moment coefficient
C_{m_q}	=	pitch damping moment coefficient due to q normalized by $qd/2V$
C_{m_α}	=	pitching moment coefficient slope
$C_{m_{\dot\alpha}}$	=	pitch damping moment coefficient due to $\dot\alpha$ normalized by $(\dot\alpha\, d/2V)$
C_N	=	normal force coefficient
C_{N_α}	=	normal force coefficient slope
C_{x0}	=	zero-yaw drag coefficient
d	=	projectile base diameter, m
F_x, F_y, F_z	=	total aerodynamic force components in inertial reference frame
K	=	turbulence kinetic energy
k	=	reduced frequency, $qd/2V$
M	=	Mach number
M_x, M_y, M_z	=	total aerodynamic moment components about mass center in inertial reference frame
p, q, r	=	components of angular velocity vector in body reference frame (roll, pitch, and yaw rates)
q	=	pitch damping moment coefficient due to q normalized by $(qd/2V)$
q^∞	=	dynamic pressure, $\frac{1}{2}\rho V^{**}2$
S	=	projectile cross-sectional area
u, v, w	=	components of velocity vector of mass center in body reference frame
V	=	magnitude of relative aerodynamic velocity vector of mass center
x, y, z	=	components of position vector of mass center in an inertial reference frame
α	=	aerodynamic angle of attack
$\dot\alpha$	=	rate of change of angle of attack
ε	=	turbulence dissipation rate
ρ	=	air density
ϕ, θ, ψ	=	Euler roll, pitch, and yaw angles

Received 21 September 2007; revision received 2 June 2008; accepted for publication 11 June 2008.

*Aerospace Engineer/Deputy Branch Chief, Aerodynamics Branch. Associate Fellow AIAA.

I. Introduction

THE prediction of aerodynamic coefficients for projectile configurations is essential in assessing the performance of new designs. Accurate determination of aerodynamics is critical to the low-cost development of new advanced guided projectiles, rockets, missiles, and smart munitions [1–3]. Although actual flight testing of advanced munitions systems will undoubtedly be an essential ingredient in the eventual success of these U.S. Army programs, it is both expensive and time consuming. Computer simulations can and have provided an effective means to determine the unsteady aerodynamics and flight mechanics of guided projectile systems. Use of high-performance computers to model, simulate, and test alternative projectile and missile designs is one response to the eventual success of new development programs. Recent advances made in high-performance computing and computational fluid dynamics (CFD) technologies have the potential for greatly reducing the design costs while providing a more detailed understanding of the complex aerodynamics than the understanding achieved through experiments and actual test firings.

For the past couple of decades, computational capabilities have been developed and used at the U.S. Army Research Laboratory for computing the flight aerodynamics of various projectile and missile configurations [4–8]. Three-dimensional steady and unsteady Navier–Stokes computational techniques have been used to predict aerodynamics of both spinning and fin-stabilized projectiles from subsonic to supersonic speeds. In many applications, 3-D Navier–Stokes computational techniques were employed in conjunction with the Chimera [9–11] overlapping grid method to model complex projectile and missile configurations. The Chimera approach was especially useful in CFD modeling of multibody projectile and missile configurations. The advanced Chimera CFD technique was then extended for accurate numerical calculation of aerodynamics involving multiple bodies with relative motion [2,3]. The underlying complex physics and fluid dynamics structure of the aerodynamic interference for multibody problems were identified. This work showed how maximum savings of time and dollars could be achieved when CFD is brought into weapon system development programs early in the design phase.

Improved computer technology and state-of-the-art numerical procedures now enable solutions to complex 3-D problems associated with projectile and missile aerodynamics. In particular, our recent focus has been directed at the development and application of advanced predictive capabilities to compute unsteady

[12,13] projectile aerodynamics. Accurate numerical modeling of the unsteady aerodynamics was found to be challenging and required the use of time-accurate solutions techniques. Recently, a time-accurate technique was used to obtain improved results for Magnus moment and roll damping moment of a spinning projectile at transonic and subsonic speeds [13]. Other recent examples have shown the use of time-accurate Navier–Stokes techniques to predict dynamic derivatives such as the pitch damping coefficient [14,15]. Recent advances made in CFD now allow one to compute both static and dynamic derivatives which, in turn, makes it possible to predict the in-flight motion of projectiles using the numerical data derived from CFD along with existing empirical and semi-empirical data. Such an approach was recently demonstrated for spin-stabilized and finned projectiles [16]. Although promising, this is a traditional approach and still requires one to determine the best aerodynamic model, and the strategy to generate the best aerodynamic models for any generalized configuration is not easily achieved. The recent advances made in the high-performance computing and unsteady CFD techniques now allow us to compute the total aerodynamic forces and moments needed in the prediction of trajectories directly. The present work is thus focused on the coupling of CFD and rigid body dynamics (RBD) techniques for simultaneous prediction of the unsteady free-flight aerodynamics and the flight trajectory of projectiles. Our goal is to be able to perform time-accurate multidisciplinary-coupled CFD/RBD computations for any projectile including the complex and unconventional ones.

Coupling of CFD and rigid body motion has been used by many researchers over the last few decades. Similar coupling strategies have been used in many areas such as multibody projectile aerodynamics [1,2], store separation problems [17–19], and others such as the prediction of helicopter hover performance [20]. The present author and his colleagues used the Chimera approach to compute time-dependent aerodynamics associated with moving multibody projectile configurations [1,2] at both supersonic and high subsonic speeds. An excellent review of the coupling of CFD and RBD for moving bodies, which also includes a description of parallel computing aspects, is given by Prewitt et al. [21]. Other examples of coupling of CFD and RBD were used by Tomaro et al. [17] and Treme et al. [18] for time-dependent store separation from an aircraft. Aircraft flowfield and store carriage loads were computed using an unstructured flow solver, and the resulting carriage loads were used in a separate 6-DOF RBD code to generate the store trajectories [17]. Treme et al. [18] used an unstructured Euler method that was tightly coupled with 6-DOF trajectory simulations. A remeshing strategy was used during the store separation process. Recently, Cheng et al. [22] have developed a set of algorithms for multidisciplinary computational fluid simulations, one of which again deals with the coupling of overset grid topology with an RBD library for simulation of relative motion between multiple bodies. RBD coupling can also be found in the area of helicopter performance prediction. Bhagwat et al. [20] have used a hybrid method that combines a vortex embedding free-wake potential technique with a viscous flow solver to predict the wake trajectories resulting from the rigid body motion of helicopter blades. The coupling of fluid flow and the movement of a rigid body such as that found in the opening and closing of valves was studied by Vierendeels et al. [23]. Although moving rigid body aerodynamics has been an area of research over the years, its use in the projectile and missile community is rather limited. Also, knowledge of the detailed aerodynamics of maneuvering guided projectiles is not easily available, especially during and after the maneuvers. Multidisciplinary computations can provide detailed fluid dynamic understanding of the unsteady aerodynamics processes involving the maneuvering flight of modern guided weapon systems. The computational technology involving CFD and RBD used in the present computational study is capable of determining the unsteady aerodynamics associated with any part of the mission trajectory of munitions, including the aerodynamic maneuvers. The present research is a big step forward in that it allows "virtual flyout" of projectiles on the supercomputers, and allows numerical prediction of the actual fight paths of a projectile and all the associated unsteady free-flight aerodynamics using coupled CFD/RBD techniques in an integrated manner.

The advanced CFD capability used here solves the Navier–Stokes equations [24] and incorporates unsteady boundary conditions and a special coupling procedure. In addition, the present research uses a body-fixed coordinate system, and the unsteady aerodynamic and flight dynamics are computed using this system, which is different from the procedures used by others for CFD and RBD coupling. The coupled procedure uses an advanced time-accurate Navier–Stokes technique capable of using both structured and unstructured methodologies. The following sections describe the solution technique, coupled CFD/RBD procedure, and the computed results obtained for a finned projectile at supersonic speeds.

II. Solution Technique

Research efforts have been ongoing to perform real-time multidisciplinary-coupled CFD/RBD computations for the flight trajectory of complex guided projectile systems. To save computer time, our earlier approach was to use a quasi-unsteady approach [4]. The quasi-unsteady approach relies on Navier–Stokes equations and 6-degree-of-freedom (6 DOF) computations to compute a missile trajectory. A degree of freedom is a displacement quantity, which defines the location and orientation of an object. In three-dimensional space, a rigid object has six degrees of freedom: three translations and three rotations. The 6-degree-of-freedom code computes linear and angular velocities as well as the orientation of the missile, which are used as input to the computational fluid dynamics code. The quasi-unsteady approach uses the following simple procedure to compute a missile trajectory. The procedure consists of the following steps:

1) A computational fluid dynamics solver repeatedly solves the Navier–Stokes equations to obtain missile flowfield solutions.

2) A sequence of average values for the forces and moments is generated from the flowfield solutions by averaging the consecutive maximum and minimum values to arrive at the forces and moments to be used as input in the 6-degree-of-freedom computations.

3) The 6-degree-of-freedom computations are performed.

4) Using the new initial conditions from the six-degree-of-freedom computations, a true increment in time is taken, and the computational fluid dynamics solver computes a new set of solutions.

These steps are repeated until the length of the desired trajectory is reached. This approach, in general, is more restrictive and may not be suitable for prediction of free-flight aerodynamics associated with unsteady maneuvers. It was not based on a body-fixed coordinate system and was only tested on a simple moving canard case [4].

Another approach that could be used is the more general real-time accurate approach. This is the preferred approach and is used in the present work. As mentioned earlier, our goal is to be able to perform time-accurate multidisciplinary-coupled CFD/RBD computations for complex guided projectiles and obtain unsteady aerodynamics associated with any part of the mission trajectory of these munitions including the aerodynamic maneuvers. The real-time accurate approach that mimics the actual free flight of these complex guided projectiles is of utmost interest to us. This approach strongly couples the CFD and the rigid body dynamics during the solution process, which is carried out in a rolling body-fixed coordinate system. It should be noted that the 6-DOF step takes only a very small fraction of the total computer time. As expected, the CFD step is the more dominate one. The real-time accurate approach requires that the 6-degree-of-freedom body dynamics be computed at each repetition or the time step of the flow solver. Details of the flow solution technique and the coupling procedure are described next.

The CFD solver used in the present work is a general purpose advanced flow solver. It solves the Navier–Stokes equations and incorporates advanced boundary conditions and grid motion capabilities. The present numerical study is a big step forward and a direct extension of that research which now includes numerical simulation of the actual fight paths of the projectile using coupled CFD/RBD techniques using the real-time accurate approach in an integrated manner. The complete set of 3-D time-dependent

Navier–Stokes equations is solved in a time-accurate manner for simulations of actual flights. A commercially available code, CFD^{++} [24–27], is used for the time-accurate unsteady CFD simulations. The basic numerical framework in the code contains unified-grid, unified-physics, and unified-computing features. The user is referred to these references for details of the basic numerical framework. The 3-D time-dependent Reynolds-averaged Navier–Stokes (RANS) equations are solved using the following finite volume method:

$$\frac{\partial}{\partial t}\int_V \mathbf{W}\,\mathrm{d}V + \oint[\mathbf{F}-\mathbf{G}]\cdot\mathrm{d}A = \int_V \mathbf{H}\,\mathrm{d}V \tag{1}$$

where $\mathbf{W}$ is the vector of conservative variables, $\mathbf{F}$ and $\mathbf{G}$ are the inviscid and viscous flux vectors, respectively, $\mathbf{H}$ is the vector of source terms, V is the cell volume, and A is the surface area of the cell face. Second-order discretization was used for the flow variables and the turbulent viscosity equation. The turbulence closure is based on topology-parameter-free formulations. Two-equation higher-order RANS turbulence models [27] were used for the computation of turbulent flows. These models are ideally suited to unstructured bookkeeping and massively parallel processing due to their independence from constraints related to the placement of boundaries and/or zonal interfaces. For computations of unsteady flowfields that are of interest here, dual time-stepping [28–30], as described next, was used to achieve the desired time accuracy. In addition, the projectile in the coupled CFD/RBD simulation, along with its grid, actually moves and rotates as it flies downrange.

A. Dual Time Stepping

The "dual-time-stepping mode" of the code was used to perform the transient flow simulations. Such procedure has been used by many researchers to obtain time-accurate solutions of unsteady flow problems [28–30]. The term "dual time step" implies the use of two time steps. The first is an "outer" or global (and physical) time step that corresponds to the time discretization of the physical time variation term. This time step can be chosen directly by the user and is typically set to a value to represent $1/100$ of the period of oscillation expected or forced in the transient flow. It is also applied to every cell and is not spatially varying.

An artificial or "inner" or local time variation term is added to the basic physical equations. This time step and corresponding "inner-iteration" strategy is chosen to help satisfy the physical transient equations to the desired degree. If the inner iterations converge, then the outer physical transient equations (or their discretization) are satisfied exactly; otherwise, they are satisfied approximately. For the inner iterations, the time step is allowed to vary spatially. Also, relaxation with multigrid (algebraic) acceleration is employed to reduce the residues of the physical transient equations. It is found that an order-of-magnitude reduction in the residues is usually sufficient to produce a good transient iteration. This may require a few internal iterations to achieve, between 3 and 10 depending on the magnitude of the outer time step, the nature of the problem, the nature of the boundary conditions, and the consistency of the mesh with respect to the physics at hand.

B. Grid Movement

Grid velocity is assigned to each mesh point. This general capability can be tailored for many specific situations. For example, the grid point velocities can be specified to correspond to a spinning projectile. In this case, the grid speeds are assigned as if the grid is attached to the projectile and spinning with it. Similarly, to account for rigid body dynamics, the grid point velocities can be set as if the grid is attached to the rigid body with 6 DOF. As shown in Fig. 1, the 6 DOF comprises the inertial position components of the projectile mass center (x, y, z) and the three standard Euler angles (ϕ, θ, ψ), roll angle, pitch angle, and yaw angle, respectively. For the rigid body dynamics, the coupling refers to the interaction between the aerodynamic forces/moments and the dynamic response of the projectile/body to these forces and moments. The forces and moments are computed every CFD time step and transferred to a 6-DOF module which computes the body's response to the forces and moments. The response is converted into translational and rotational accelerations that are integrated to obtain translational and rotational velocities and integrated once more to obtain linear position and angular orientation. The 6-DOF rigid body dynamics module uses quaternions to define the angular orientations. However, these are easily translated into Euler angles. From the dynamic response, the grid point locations and grid point velocities are set.

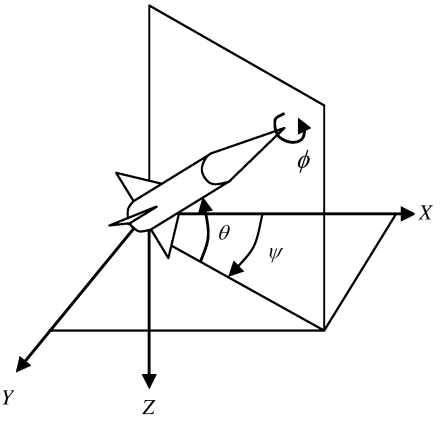

Fig. 1 Six-degree-of-freedom schematic.

C. Six Degree-of-Freedom Coupling

The actual coupling between CFD and the 6-DOF module is similar to that used by others [21–23]. What is unique here is that the coupled calculations are performed in a body-fixed coordinate system. In addition, the procedure to start the coupled calculations is quite unique in itself, as described next. Here, two modes are available to help simulate rigid body dynamics: an uncoupled mode and a coupled mode. The coupling refers to the interaction between the aerodynamic forces/moments and the dynamic response of the projectile/body to these forces and moments. In both modes, the forces and moments are computed every time step and reported to the user. In the coupled mode, the forces and moments are passed on to a 6-DOF module which computes the body's response to the forces and moments. The response is converted into translational and rotational accelerations, which are integrated to result in translational and rotational velocities, and integrated once more to result in linear position and angular orientation. The 6-DOF rigid body dynamics module uses quaternions to define the angular orientations. However, these are easily translated into Euler angles. From the dynamic response, the grid point locations and grid point velocities are set. In the uncoupled mode, the forces and moments are not coupled with the rigid body dynamics module. The motion of the projectile is kinematics only and depends on the initial linear and angular velocities prescribed.

The projectile state vector is composed of the inertial position components of the projectile mass center (x, y, z), the standard Euler angles (ϕ, θ, ψ), the body frame components of the projectile mass center velocity (u, v, w), and the body frame components of the projectile angular velocity vector (p, q, r). The entire state vector consisting of these 12 variables is required in the initial conditions before a virtual flyout can be performed and a coupled dynamic solution can be obtained. Typically, we begin with a computation performed in "steady-state mode" with the grid velocities prescribed to account only for the translational motion component of the complete set of initial conditions to be prescribed. At this stage, we also impose the angular orientations from the initial conditions. The complete set of initial conditions includes both translational and rotational velocity components, along with initial position and angular orientation. With a fixed translational velocity, we obtain the steady-state solution. This becomes the initial condition for the next step, which involves adding just the spin component of the projectile. With the addition of spin, time-accurate calculations are performed

for a few cycles of spin until converged periodic forces and moments are obtained. A sufficient number of time steps are performed so that the angular orientation for the spin axis corresponds to the prescribed initial conditions. All this is performed in an uncoupled mode. The angular velocity initial conditions associated with the nonspin rotational modes are then added. The mesh is translated back to the desired initial position, the nonspin rotational velocity initial conditions are turned on, and computations are carried out in the coupled mode.

III. Results

Time-accurate unsteady numerical computations were performed using Navier–Stokes and coupled 6-DOF methods to predict the unsteady flowfields, aerodynamic coefficients, and flight paths of a finned projectile at supersonic speeds. In all cases, full 3-D computations were performed and no symmetry was used.

The supersonic projectile modeled in this study is an ogive-cylinder-finned configuration (see Fig. 2). The length of the projectile is 121 mm and the diameter is 13 mm. The ogive nose is 98.6 mm long and the afterbody has a 22.4 mm, 2.5 deg boattail. Four fins are located on the back end of the projectile. The fins have a thickness of 1.02 mm, a sweep angle of approximately 30 deg, a 25 mm span, a 22.3 mm root chord, and a 10.3 mm tip chord. The fins have the same constant thickness everywhere, including the leading and trailing edges. The center of gravity of the projectile is located 57.34 mm from the nose. The computational mesh for the 25-mm projectile model is a C-grid (see Fig. 3) consisting of seven zones. The first zone encompasses the entire projectile body, from the tip of the nose to the end of the fins. In general, most of the grid points are clustered in the afterbody fin region. Figure 3 shows a 3-D view of the full projectile mesh. The total number of grid points is 4 million for the full computational grid shown here. Figure 4 shows an expanded view of the grid in the base region. The first grid point spacing from the projectile body is chosen to achieve a $y+$ value of 1.0. Grid sizes were varied from a total of 2, 4, and 6 million points using structured hexahedral grids. For the larger meshes, additional grid points were included in the fin and the near-wake regions. In addition, an unstructured grid (see Fig. 5) was also obtained which also modeled a cavity that was present in the actual configuration tested. Again, most of the grid points in this case are also clustered in the boundary layer, as well as near the afterbody fin and the wake regions. The total number of grid points is about 6 million for the full grid. Only the unstructured mesh included the base cavity region and was generated using the Multipurpose Intelligent Meshing Environment (MIME) grid-generation software recently developed by Metacomp Technologies. Results obtained from different grids are discussed later in this section.

Here, the primary interest is in the development and application of coupled CFD and RBD techniques for accurate simulation of the free-flight aerodynamics and flight dynamics of the projectile in supersonic flight. The first step here was to obtain the steady-state results for this projectile at a given initial supersonic velocity. Also imposed were the angular orientations at this stage. A corresponding converged steady-state solution was then used as the starting condition, along with the other initial conditions for the computation of coupled CFD/RBD runs. Numerical computations have been made for these cases at initial velocities of 1037 and 1034 m/s,

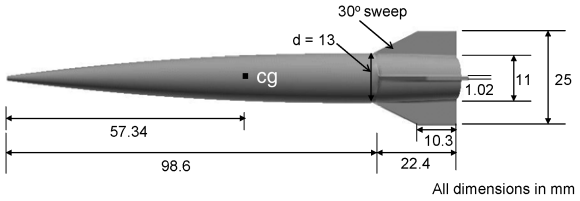

Fig. 2 Finned projectile configuration.

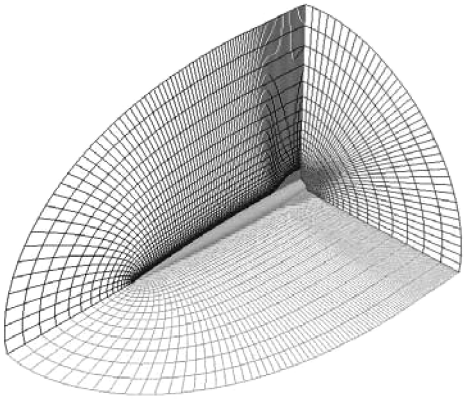

Fig. 3 Computational grid near the projectile.

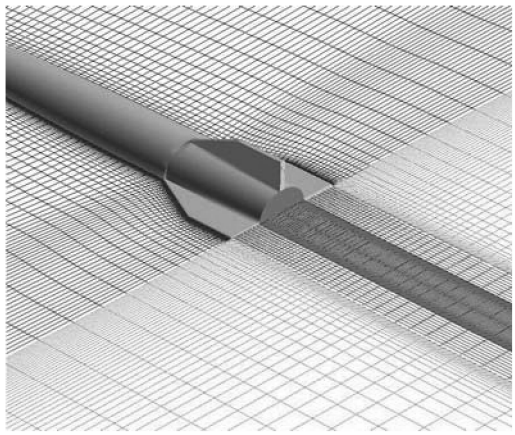

Fig. 4 Expanded view of the grid in the base region.

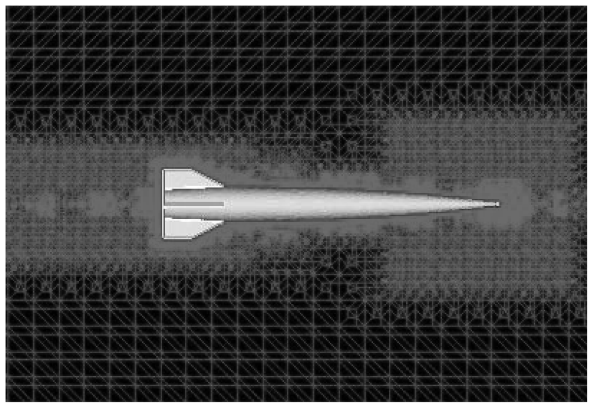

Fig. 5 Unstructured mesh near the finned body.

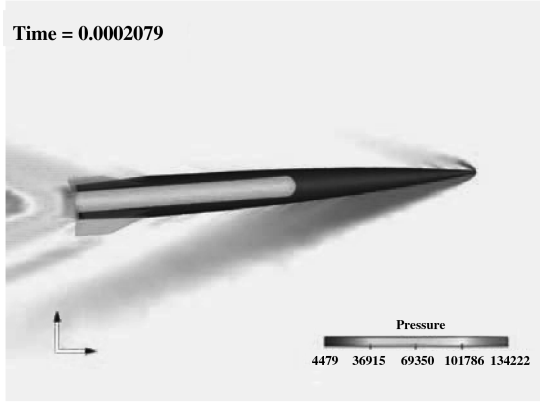

Fig. 6 Computed pressure contours.

depending on whether the simulations were started from the muzzle or a small distance away from it. The corresponding initial angles of attack were $\alpha = 0.5$ or 4.9 deg, and initial spin rates were 2800 or 2500 rad/s, respectively. The initial conditions at the first station were obtained as part of the fitting procedure of the actual flight data using ARFDAS [31]. The other set of initial conditions start at the muzzle itself and are somewhat more arbitrary. In either simulation, CFD provided the total aerodynamic forces and moments for the computed flight trajectories. Figure 6 shows the computed pressure contours at a given time or at a given location in the trajectory. It clearly shows the orientation of the body at that instant in time and the resulting asymmetric flowfield due to the body at angle of attack. Of course, the orientation of the projectile changes from one instant in time to another as the projectile flies down range.

Figures 7 and 8 show the computed z and y distances as a function of x (or, the range). The computed results are shown in solid lines and are compared with the data measured from actual flight tests. For the computed results, the aerodynamic forces and moments were completely obtained through CFD. One simulation started from the gun muzzle and the other from the first station (referred to here as FS) away from the muzzle where the actual data was measured. The first station was located about 0.9 m from the muzzle. Both sets of results are generally found to be in good agreement with the measured data, although there is a small discrepancy between the two sets of computed results. Initially, the computed trajectories obtained using both initial conditions match well with the flight data and then they seem to diverge. The computed results even at higher x distances (60 m and up) are still within a few percent from the measured data. Although not shown here, the trajectory from the ARFDAS fitting procedure does goes through the data because they were fitted as such. Both y and z distances are found to increase with increasing x distance.

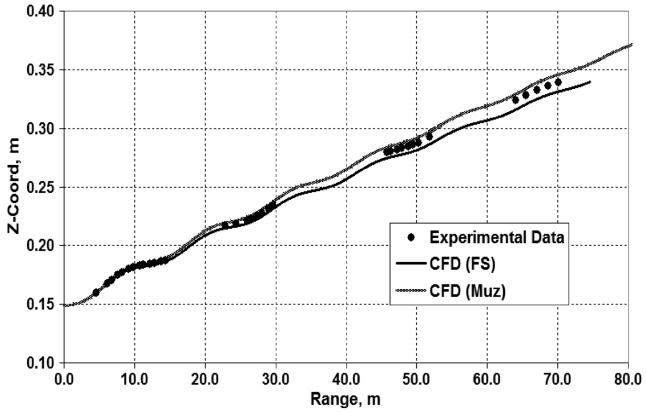

Fig. 7 Computed z distance vs range.

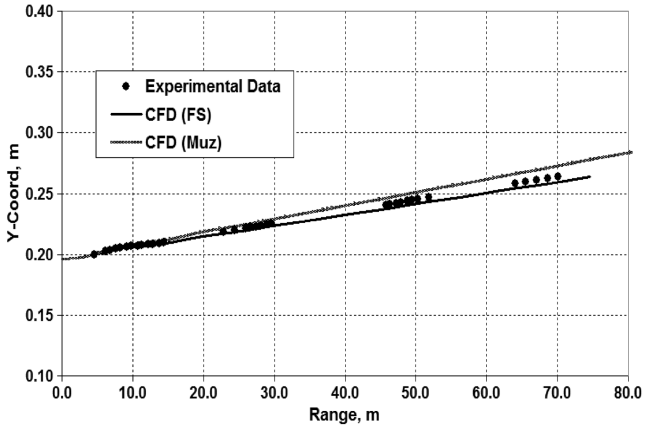

Fig. 8 Computed y distance vs range.

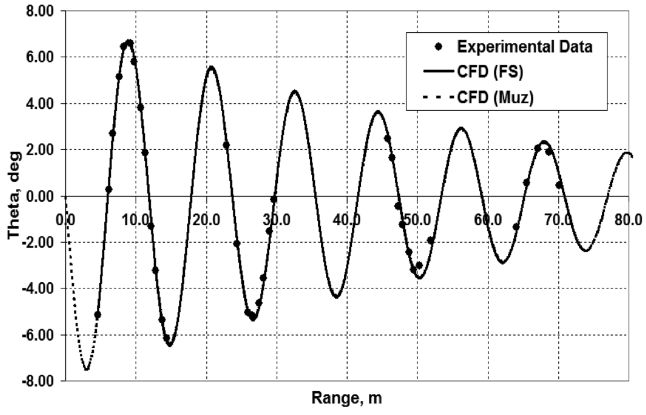

Fig. 9 Euler pitch angle vs range.

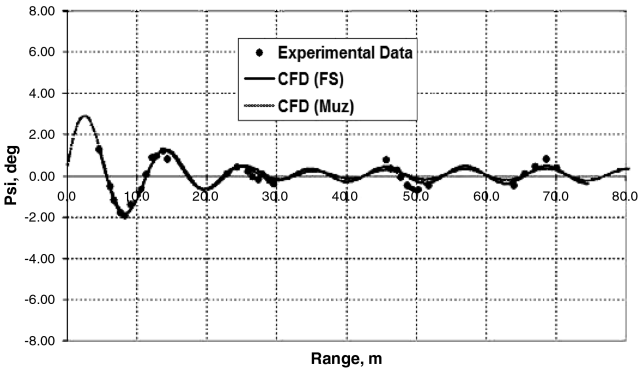

Fig. 10 Euler yaw angle vs range.

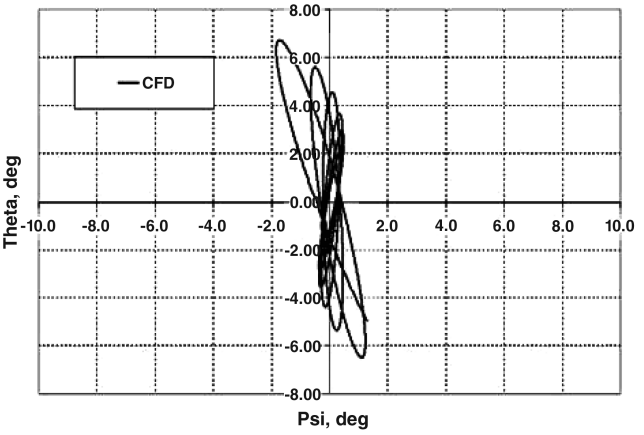

a)

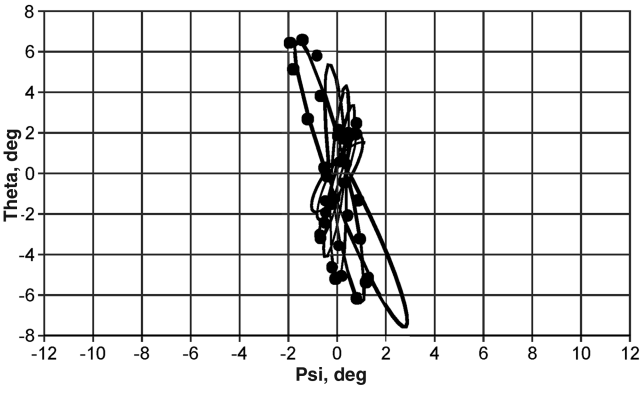

b)

Fig. 11 Motion plot a) computation, b) flight test.

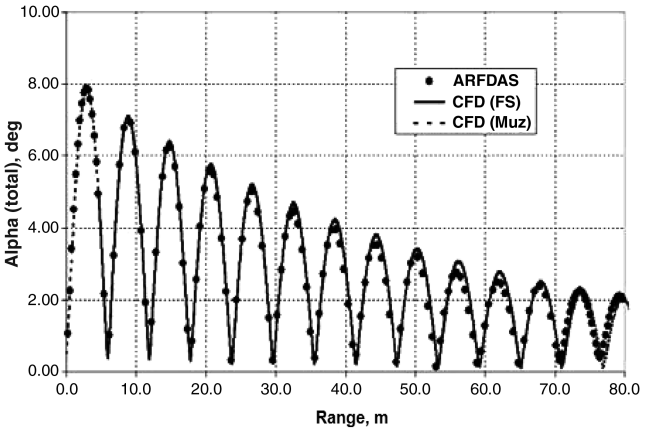

Fig. 12 Total angle of attack vs range.

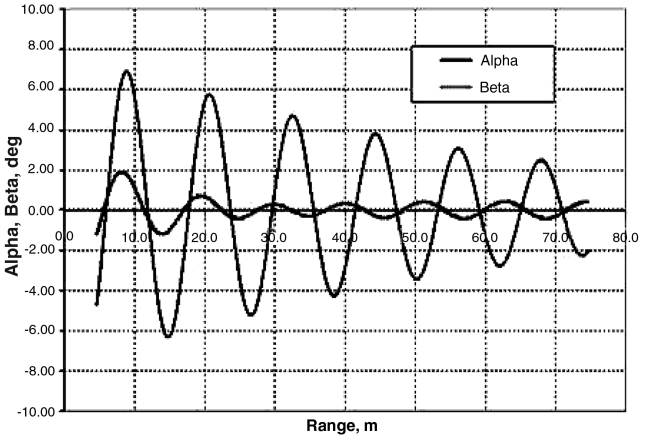

Fig. 13 Angle of attack and side slip vs range.

Figure 9 shows the variation of the Euler pitch angle with distance traveled. As seen in this figure, both the amplitude and frequency in the Euler pitch angle variation are predicted very well by the computed results and match extremely well with the data from the flight tests. Both sets of computations, whether started from the muzzle or the first station away from the muzzle, yield essentially the same results. One can also clearly see the amplitude damped out as the projectile flies down range, that is, with increasing x distance. Figure 10 shows similar behavior with Euler yaw angle with x distance. In this case, however, the yaw angle damps out somewhat in the beginning up to the 20 m range, and then the amplitude stays within $+0.5$ and -0.5 deg for the rest of the flight. The computed results again compare very well with the measured data from the flight tests.

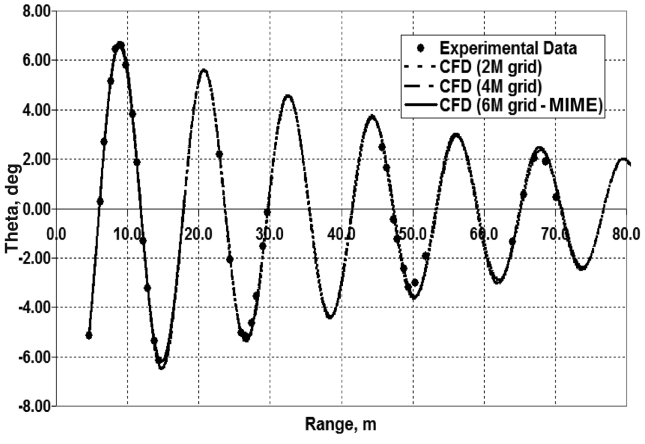

Fig. 14 Effect of mesh size and type on the Euler pitch angle.

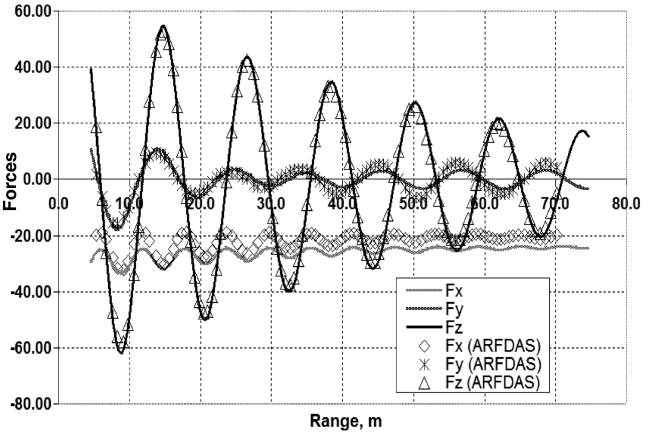

Fig. 15 Comparison of Earth-fixed aerodynamic forces.

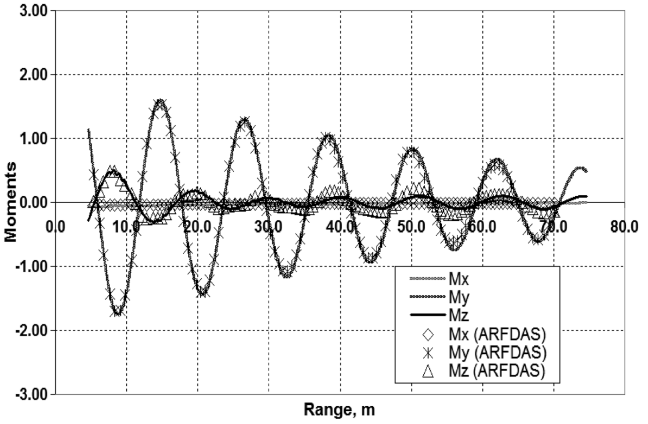

Fig. 16 Comparison of Earth-fixed aerodynamic moments.

The time histories of the pitch and yaw angles are often customarily presented as a motion plot where the pitch angle is plotted versus the yaw angle during the flight of the projectile. It represents the path traversed by the nose of the projectile during the flight trajectory (looking forward from the back of the projectile). Such a plot is shown in Fig. 11. This figure shows the comparison of the motion plots obtained both from the numerical simulations and the 6-DOF analysis of the flight results from ARFDAS [31]. Computed results match very well with the experimental flight test results. Figures 12 and 13 show the computed total angle of attack and the individual components (angle of attack and side slip), respectively, as a function of the range. These quantities are not directly measured in the actual tests. However, they can be easily derived from the "6-DOF fits" of the actual data. Figure 12 shows the

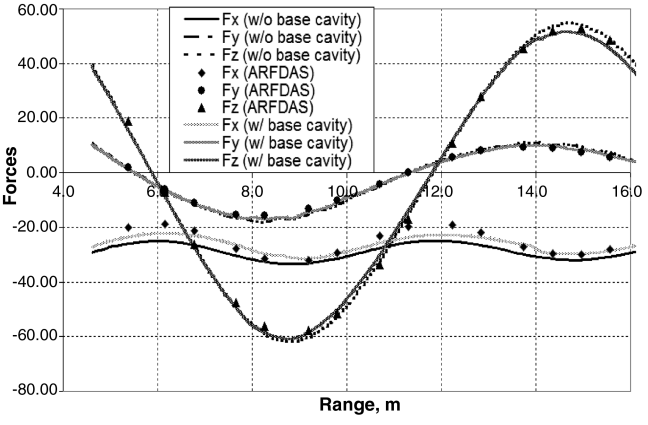

Fig. 17 Aerodynamic forces vs x distance.

Table 1 Comparison of extracted aerodynamic coefficients with test data

Data source	Mach no.	Axial force coeff., C_{x0}	Normal force coeff. deriv., C_{N_α}	Pitching moment coeff. deriv., C_{m_α}	Pitch damping moment coeff., C_{m_q}	Roll damping moment coeff., C_{lp}
Spark range	3.0	0.22	5.83	−12.60	−196	−2.71
CFD (1)	3.0	0.24	5.88	−12.46	−172	−3.24
CFD (2)	3.0	0.24	5.83	−12.36	−150	−3.40

comparison of the total angle of attack derived from such an analysis with the computed results. Computed results include two simulations with different starting conditions, and both sets of these results match quite well with the data derived from the usual 6-DOF fits. All results show the total angle of attack decreasing with increasing range or x distance. Figure 13 shows the both component angles: angle of attack and the side slip.

As stated earlier, different computational meshes were used to obtain the numerical results. Both structured and unstructured grids were generated. In addition, different grid sizes of 2 and 4 million mesh points were used with the structured hexahedral grids. Figure 14 shows the computed Euler angles as a function of distance and, as shown in this figure, the results obtained with 4 million point mesh produces essentially the same results obtained with the 2 million point mesh. Additionally, the same solution is obtained irrespective of whether structured or unstructured grids are used. Another factor that can affect the accuracy of the computed results is the time step used in the computations. Two different time steps of 0.787e-05 s and 0.696e-06 s were used. Although not shown here, the computed results changed very little when the time step used was reduced by a factor of 3.

Figures 15 and 16, respectively, show the comparison of the predicted aerodynamic forces and moments with the ARFDAS results for the same flight conditions. The aerodynamic forces are shown in three directions: x (down range), y (cross range, positive to the left looking from the gun), and z (altitude, positive up). The same sign conventions used in ARFDAS are used in the present study. The moments in this case are taken with respect to the center of gravity of the projectile. As seen in these figures, both the predicted unsteady forces and moments have very similar behavior to that used in the 6-DOF analysis of the actual flight test data. The aerodynamic forces in the y and z directions match well with their counterparts in the ARFDAS analysis. However, there is clearly a discrepancy in the comparison of the aerodynamic force in the x direction. Because the drag acts in the negative x direction, the computed drag is overpredicted by 20–25%. Although not shown here, a finer grid was used in the steady-state mode and the drag results did not change appreciably. Another source of error could come from the inaccurate modeling of the model itself. The actual flight model did have a cavity in the base region. A part of the discrepancy can perhaps be attributed to this. As seen in Fig. 16, the aerodynamic moments are generally found to be in good agreement with the aerodynamic moments used in ARFDAS.

The actual flight model included a base cavity which is known to have an effect on the aerodynamic axial force. In the present computations, using the unstructured grid, the base cavity was modeled and the flowfield inside the base cavity was computed. Figure 17 shows the total aerodynamic forces in the three coordinate directions. This figure shows the comparison of these forces both with and without the base cavity with the forces obtained from ARFDAS. As expected, the force in x direction F_x is affected due to the cavity. The predicted F_x obtained with the base cavity matches with the ARFDAS result better than the F_x predicted without it. The difference between the ARFDAS result and the computed result without the base cavity is almost zero in some parts of the drag cycle (e.g., x distance between 8 and 10 m) and the maximum deviation is as high as 30%. With the base cavity modeled, the maximum deviation drops to less than 15%. The base cavity appears to have a negligible effect on the other aerodynamic forces.

The results produced by the virtual flyout simulations provide the total aerodynamic forces and moments at every time step as the projectile flies down range. For a variety of reasons, one may want to extract the traditional aerodynamic force and moment coefficients from these coupled CFD/RBD simulations. For example, the aerodynamic coefficients are in many cases available from experiments and other databases and can be used for further verification and validation of the computed results obtained from the virtual flyout simulations. Currently, work is in progress to look at a number of ways to achieve it. One way is to feed the CFD/RBD generated data back into software such as ARFDAS and back out the aerodynamic coefficients with the same procedure used on the actual test data.[†] Another approach is to perform a set of short time histories or virtual flyouts at different Mach numbers and use a simple fitting procedure to estimate all aerodynamic force and moment coefficients [32].

Both approaches were used in this study to extract the aerodynamic force and moment coefficients for the finned projectile. In the first approach, the position (x, y, and z) and the orientation (three Euler angles) of the projectile, obtained from the virtual flyout simulations, were provided as input to ARFDAS. These are the six quantities that are actually measured in the free-flight tests, a reduction procedure is carried out, and the aerodynamics that best fit the data are obtained. The CFD generated data were cast to resemble spark range data and the same fitting procedure was applied. The aerodynamics that matched the CFD supplied data were obtained and the aerodynamic coefficients extracted.[†] The second approach [32] is currently being developed and the results, although somewhat preliminary, are included for comparison. This approach does not use the ARFDAS fitting technique and therefore provides for an alternate way to get extract the aerodynamic coefficients from the same simulation. It uses another fitting procedure to efficiently generate a complete aerodynamic model using short time histories of virtual flyout simulations. The extracted aerodynamic coefficients are shown in Table 1 and are compared with the same coefficients obtained using the actual test data. As shown in Table 1, computed static aerodynamic coefficients are generally in good agreement and are within 9, 0.8, and 1.9% of the data for the drag coefficient, normal force coefficient, and pitching moment coefficient, respectively. The table also includes comparison of the dynamic derivatives such as the pitch damping moment and the roll damping derivatives. Dynamic derivatives extracted by the first approach seem to be in slightly better agreement (within 12%) with the data than those extracted by the second approach (within 23%). Computed pitch damping moment and roll damping moment coefficients predicted by the first approach are within 12 and 23% of the data, respectively, and the deviation increases to 19 and 25%, respectively, with the second approach. As stated earlier, the second approach is still under development and its accuracy is expected to improve in the near future.

IV. Conclusions

This article describes a new coupled CFD/RBD computational study undertaken to simultaneously determine the flight trajectory and the associated unsteady free-flight aerodynamics of a finned projectile. A three-dimensional unsteady Navier–Stokes solver is employed to compute the time-accurate aerodynamics associated with the free flight of the finned projectile at supersonic velocities. Computed positions and orientations of the projectile have been

[†]Wayne, H., Private Communications, Arrow Tech Associates, South Burlington, VT, June 2007.

compared with actual data measured from free-flight tests and are found to be generally in very good agreement. Predicted aerodynamics forces and moments also compare generally well with the forces and moments used in the 6-DOF fits of the results of the same tests. There was some discrepancy between the predicted axial force and the axial force obtained from the 6-DOF fit of the flight data. To improve the accuracy of predicted axial force, the base cavity that was present in the actual model was included in the computations. The computed results obtained with the base cavity matched better with the data than the predicted axial force without the cavity.

Different approaches of extracting traditional aerodynamic coefficient data were discussed and used to extract these coefficients from the new virtual flyout simulations. The extracted aerodynamic coefficients from the virtual flyout match quite well with the aerodynamic coefficients obtained from the 6-DOF fits of the actual flight test data. This further validates the accuracy of the computed results obtained form the virtual flyouts. Future work will include extending the virtual flyout technique to subsonic and transonic speeds. Research efforts will continue with the validation of the computed results with the data, results from other techniques, and extraction of the aerodynamic coefficients from the simulations at hand for other geometries and flight conditions.

This work demonstrates a coupled method to accurately predict the time-accurate unsteady aerodynamics and the flight trajectories of projectiles at various speeds. The present CFD/RBD simulations and comparison of the computed results with the data clearly demonstrate the applicability of the current method. The current method is equally applicable to complex configurations and other speed regimes, such as subsonic and transonic flights. The true power of the method lies in its application and analysis to configurations with nonlinear aerodynamics and/or transonic speed regime and thus forms the basis for future multidisciplinary, time-dependent computations of advanced maneuvering munitions.

Acknowledgments

This work was accomplished as part of a grand challenge project jointly sponsored by the U.S. Department of Defense High-Performance Computing Modernization program and the U.S. Army Research Laboratory. The author wishes to thank Sukumar Chakravarthy of the Metacomp Technologies for his technical assistance on some of the issues on the coupling techniques between computational fluid dynamics and rigid body dynamics. The author also wishes to thank Wayne Hathaway of Arrow Tech Associates for providing expert advice and help with the 6-degree-of-freedom simulations with their software, ARFDAS. The scientific visualization and the computational support of the Army Research Laboratory Major Shared Resource Center are greatly appreciated.

References

[1] Sahu, J., Heavey, K. R., and Ferry, E. N., "Computational Modeling of Multibody Aerodynamic Interference," *Advances in Engineering Software*, Vol. 29, Nos. 3–6, April 1998, pp. 383–388. doi:10.1016/S0965-9978(98)00004-0

[2] Sahu, J., and Nietubicz, C. J., "Application of Chimera Technique to Projectiles in Relative Motion," *Journal of Spacecraft and Rockets*, Vol. 32, No. 5, Sept.–Oct. 1995, pp. 795–800. doi:10.2514/3.26686

[3] Meakin, R. L., "Computations of the Unsteady Flow About a Generic Wing/Pylon/Finned-Store Configuration," AIAA Paper 92-4568-CP, Aug. 1992.

[4] Sahu, J., Edge, H. L., DeSpirito, J., Heavey, K. R., Ramakrishnan, S. V., and Dinavahi, S. P. G., "Applications of Computational Fluid Dynamics to Advanced Guided Munitions," *39th AIAA Aerospace Sciences Meeting*, AIAA Paper 2001-0799, Jan. 2001.

[5] Sahu, J., Edge, H. L., Dinavahi, S., and Soni, B., "Progress on Unsteady Aerodynamics of Maneuvering Munitions," *Users Group Meeting Proceedings*, June 2000.

[6] Silton, S. I., "Navier–Stokes Computations for a Spinning Projectile for Subsonic to Supersonic Speeds," *Journal of Spacecraft and Rockets*, Vol. 42, No. 2, 2005, pp. 223–231. doi:10.2514/1.4175

[7] Heavey, K. R., and Sahu, J., "Application of Computational Fluid Dynamics to a Monoplane Fixed-Wing Missile with Elliptic Cross-Sections," ARL TR-3549, July 2005.

[8] Sahu, J., Silton, S. I., and Heavey, K. R., "Navier–Stokes Computations of Supersonic Flow over Complex Missile Configurations," *AIAA 22nd Applied Aerodynamics Conference*, AIAA Paper No. 2004-5456, Aug. 2004.

[9] Steger, J. L., Dougherty, F. C., and Benek, J. A., "A Chimera Grid Scheme," *Advances in Grid Generation*, edited by K. N. Ghia, and U. Ghia, American Society of Mechanical Engineers, Fluids Engineering Div.-5, Fairfield, NJ, June 1983, pp. 59–69.

[10] Meakin, R., and Gomez, R., "On Adaptive Refinement and Overset Structured Grids," AIAA Paper No. 97-1858-CP, 1997.

[11] Meakin, R., "Unsteady Simulation of the Viscous Flow About a V-22 Rotor and Wing in Hover," AIAA Paper 95-3463, Aug. 1995.

[12] Sahu, J., "Unsteady CFD Modeling of Aerodynamic Flow Control over a Spinning Body with Synthetic Jet," AIAA Paper 2004-0747, Jan. 2004.

[13] DeSpirito, J., and Heavey, K. R., "CFD Computation of Magnus Moment and Roll Damping Moment of a Spinning Projectile," *Atmospheric Flight Mechanics Conference*, AIAA Paper No. 2004-4713, Aug. 2004.

[14] Oktay, E., and Akay, H. U., "CFD Predictions of Dynamic Derivatives for Missiles," AIAA Paper No. 2002-0276, Jan. 2002.

[15] Park, S. H., and Kwon, J. H., "Navier–Stokes Computations of Stability Derivatives for Symmetric Projectiles," AIAA Paper No. 2004-0014, Jan. 2004.

[16] Dietrich, F., Guillen, P., and Cayzac, R., "A Flight Mechanics/Aerodynamics Coupling Methodology for Projectiles," AIAA Paper No. 2003-29, Jan. 2003.

[17] Tomaro, R. F., Witzeman, F. C., and Strang, W. Z., "Simulation of Store Separation for the F/A-18-C Using Cobalt(60)," *Journal of Aircraft*, Vol. 37, No. 3, May–June 2000, pp. 361–367.

[18] Treme, U., Hitzel, S. M., Sorensen, K. A., and Weatherhill, N., "JDAM-Store Separation from an F/A-18-C: An Application of the Multidisciplinary SimServer-System," *23rd AIAA Applied Aerodynamics Conference*, AIAA Paper 2005-5222, June 2005.

[19] Harish, G., Pavankumar, M., and Anandhanarayan, K., "Store Separation Dynamics Using Grid-Free Euler Solver," *24th AIAA Applied Aerodynamics Conference*, AIAA Paper 2006-3650, June 2006.

[20] Bhagwat, M. J., Moulton, M. A., and Caradonna, F. X., "Development of a CFD-Based Hover Performance Prediction Tool for Engineering Analysis," *Journal of the American Helicopter Society*, Vol. 52, No. 3, July 2007, pp. 175–188.

[21] Prewitt, N. C., Belk, D. M., and Shyy, W., "Parallel Computing Overset Grids for Aerodynamic Problems with Moving Objects," *Progress in Aerospace Sciences*, Vol. 36, No. 2, Feb. 2000, pp. 117–172. doi:10.1016/S0376-0421(99)00013-5

[22] Cheng, G. C., Koomullil, R. P., and Soni, B. K., "Multidisciplinary and Multi-Scale Computational Field Simulations: Algorithms and Applications," *Mathematics and Computers in Simulation*, Vol. 75, Nos. 5–6, 2007, pp. 161–170. doi:10.1016/j.matcom.2006.12.007

[23] Vierendeels, J., Dumont, K., Dick, E., and Verdonck, P., "Analysis and Stabilization of Fluid-Structure Interaction Algorithm for Rigid-Body Motion," *AIAA Journal*, Vol. 43, No. 12, Dec. 2005, pp. 2549–2557. doi:10.2514/1.3660

[24] Peroomian, O., Chakravarthy, S., and Goldberg, U., "A 'Grid-Transparent' Methodology for CFD," AIAA Paper 97-07245, 1997.

[25] Batten, P., Goldberg, U., and Chakravarthy, S., "Sub-Grid Turbulence Modeling for Unsteady Flow with Acoustic Resonance," *38th AIAA Aerospace Sciences Meeting*, AIAA Paper 00-0473, Jan. 2000.

[26] Peroomian, O., Chakravarthy, S., Palaniswamy, S., and Goldberg, U., "Convergence Acceleration for Unified-Grid Formulation Using Preconditioned Implicit Relaxation," AIAA Paper 98-0116, 1998.

[27] Goldberg, U. C., Peroomian, O., and Chakravarthy, S., "A Wall-Distance-Free K-E Model with Enhanced Near-Wall Treatment," *Journal of Fluids Engineering*, Vol. 120, No. 3, 1998, pp. 457–462. doi:10.1115/1.2820684

[28] Tsai, H. M., Wong, A. S. F., and Cai, J., "Unsteady Flow Calculations with a Parallel Multiblock Moving Mesh Algorithm," *AIAA Journal*, Vol. 39, No. 6, June 2001, pp. 1021–1029.

[29] Zhang, L. P., and Wang, Z. J., "A Block LU-SGS Implicit Dual Time-Stepping Algorithm for Hybrid Dynamic Meshes," *Computers and Fluids*, Vol. 33, No. 7, Aug. 2004, pp. 891–916. doi:10.1016/j.compfluid.2003.10.004

[30] Gilmanov, A., and Sotiropolous, F., "A Hybrid Cartesian/Immersed Boundary Method for Simulating Flows with 3-D, Geometrically Complex, Moving Bodies," *Journal of Computational Physics*,

Vol. 207, No. 2, Aug. 2005, pp. 457–492.
doi:10.1016/j.jcp.2005.01.020
[31] "ARFDAS Technical Manual," Arrow Tech Associates, South Burlington, VT, 2001.
[32] Kokes, J., Costello, M., and Sahu, J., "Generating an Aerodynamic Model for Projectile Flight Simulation Using Unsteady Time Accurate Computational Fluid Dynamic Results," U.S. Air Force Research Lab. CR-577, Sept. 2006.

M. Costello
Associate Editor